Vol. 62: 25–43, 2014
doi: 10.3354/cr01262

CLIMATE RESEARCH
Clim Res

Published online December 2

Sensitivity of regional climate simulations to land-surface schemes on the Tibetan Plateau

Xuejia Wang[1,3], Meixue Yang[1,*], Guojin Pang[2]

[1]State Key Laboratory of Cryospheric Sciences and [2]Laboratory of Remote Sensing and Geospatial Science, Cold and Arid Regions Environmental and Engineering Research Institute, Chinese Academy of Sciences, Lanzhou Gansu 730000, PR China
[3]University of Chinese Academy of Sciences, Beijing 100049, PR China

ABSTRACT: To investigate the effects of land-surface schemes in 2 regional climate models (RegCM3 and RegCM4.3.4) on the Tibetan Plateau (TP) climate simulation, 3 groups of 10 yr (1992–2001) simulation experiments were performed based on 2 land-surface schemes (BATS and CLM3.5). The simulations (RegCM3_BATS, RegCM4_BATS, and RegCM4_CLM) were compared with observed data by setting the same domain and initial and lateral atmospheric boundary conditions and using 30 km spatial resolution. The results showed that, compared to observed data, regional average annual mean temperature was underestimated by 1.22, 2.11, and 1.32°C, and regional average annual precipitation was overestimated by 43.2, 49.8, and 18.4% in RegCM3_BATS, RegCM4_BATS, and RegCM4_CLM respectively. There were significant differences in simulated energy and water budget components among the 3 models resulting from the influence of the 2 different land-surface parameterization schemes, which impacted the simulated precipitation and temperature results through interaction between the land surface and the atmosphere. Therefore, climate simulation over the TP is very sensitive to the use of different land-surface schemes in regional climate models. Overall, use of RegCM4_CLM instead of RegCM_BATS resulted in a warmer and drier land surface and a better simulation of annual average spatial patterns of temperature and precipitation.

KEY WORDS: Tibetan Plateau · Regional climate model · Land-surface scheme · Temperature · Precipitation

1. INTRODUCTION

As the highest and largest plateau in the world, the Tibetan Plateau (TP), known as the 'third polar region', directly impacts its surrounding climate system and environment through its thermal and dynamical effects (e.g. Ye 1979, Wu et al. 2012, Yao et al. 2012). Land-surface processes are a very important component of climate systems and include thermal, hydrological, and biological processes and land-atmosphere exchanges of energy and matter (Wang 1999). The land surface represents the lower atmospheric boundary condition for approximately 30% of the Earth's surface. Water and energy exchange between ground and atmosphere occurs mainly at this interface. Climate over the TP is influenced by the Asian monsoon, and the land-surface processes which regulate seasonal heating are probably responsible to some extent for interannual monsoon variability. Snow cover and soil moisture anomalies over the Eurasian continent in pre-monsoon seasons are thought to have a large impact on Asian summer monsoon variability (Yasunari 2006). Freezing and thawing processes at the soil surface have a significant effect on the nature of plateau land–atmosphere interactions (Yang et al. 2007a, Guo et al. 2011). One of the effects of soil on weather and climate is evaporation of soil water (Yang et al. 2007b). Zhang et al. (2011) found that soil moisture exerts a substantially stronger impact on daily maximum temperature vari-

*Corresponding author: mxyang@lzb.ac.cn

ability than on daily mean temperature over China. Land–atmosphere coupling mainly amplifies hot extremes over China (Zhang & Wu 2011). Overall, land–atmosphere interactions have a substantial impact on energy exchange processes and water distribution, and even on climate change.

Permafrost, seasonally frozen soil, snow cover, alpine meadows, grasslands, and alpine deserts are widely distributed on the TP. Frequent exchanges of matter, energy, and momentum occur between different underlying surfaces and the atmosphere. Thus, land–atmosphere interactions over the TP are intense and complex (Ma et al. 2009). For this reason, study of land-surface parameterization schemes on the TP is particularly important. In recent years, numerical simulation has been more widely used in climate research, reflecting the development of computation skills and improved understanding of climate system components and their interactions. As a form of numerical simulation, high-resolution regional climate models have emerged as a valuable tool to understand regional climate characteristics and change and to elucidate the mechanisms involved (e.g. Giorgi et al. 1990, 1993a, 1993b, Wang et al. 2004 and references therein, Pal et al. 2007, Laprise 2008, Li & Xue 2010, Giorgi et al. 2012, Wang et al. 2013). Various versions of the RegCM regional climate model have been applied to many regions throughout Asia, for example in East and South Asia (Liu et al. 1994, Lee & Suh 2000, Gao et al. 2002, Dash et al. 2006, Ju & Wang 2006, Ju et al. 2007, Phan et al. 2009, Octaviani & Manomaiphiboon 2011, Gu et al. 2012, Park et al. 2013), in China (Gao et al. 2001, 2011, Shi et al. 2011), and on the TP (Zhang et al. 2005, Qu et al. 2009, Ji & Kang 2013, Wang et al. 2013). Some sensitivity tests with respect to cumulus cloud parameterization schemes (Yang & Yang 2008), boundary conditions (Park et al. 2013), and land-surface schemes elsewhere than on the TP (Zou & Xie 2012, Chen et al. 2012) have been carried out. Wang et al. (2013) presented a 20 yr (1982–2001) climate simulation using RegCM3 over the TP and compared RegCM3 and RegCM4, using the Community Land Model version 3.5 (CLM3.5) land-surface scheme, for a 1 yr simulation. However, only temperature and precipitation were involved in these comparisons. Further comparisons, including longer-time-scale simulations and more output variables, are therefore needed in order to identify an appropriate land-surface scheme for climate simulation on the TP.

In this study, the same experimental domain, initial and lateral boundary conditions, and horizontal resolution were configured and used with the 2 versions of the RegCM regional climate model (RegCM3 and RegCM4.3.4) and the 2 available land-surface schemes, CLM3.5 and the Biosphere-Atmosphere Transfer Scheme (BATS), to conduct 3 groups of 10 yr numerical experiments (1992–2001), drawing on the results of previous work. Analysis of the influence of different land-surface schemes on TP climate simulation can provide valuable guidance for improvement of land-surface process schemes, thereby helping to reduce the uncertainties of physical process description and to optimize TP climate simulation.

Section 2 introduces the RegCM regional climate model and the experimental design and data used in this study. The results are presented and discussed in Section 3, and Section 4 summarizes the conclusions.

2. MODEL AND EXPERIMENTAL DESIGN

2.1. Descriptions of land-surface models

The differences between the 2 land-surface models used in this study are shown in Table 1. BATS includes a 1-layer vegetation module, a 1-layer snow module, and a 3-layer soil scheme (a 10 cm-thick surface soil layer, a 1 to 2 m thick root-zone layer, and a 3 m deep soil layer). Twenty land-cover and vegetation types from the Global Land Cover Characterization (GLCC) datasets were used in BATS to determine surface properties like albedo, roughness, and moisture for each grid point. Predictive equations were solved for soil-layer temperatures using a generalization of the Deardoff (1978) force-restore method. Soil hydrology calculations included predictive equations for soil-layer water content. A mosaic-type parameterization of subgrid-scale topography and land use was implemented. The parameterization used a regular fine-scale surface subgrid for each coarse-model grid cell (Giorgi et al. 2003). Surface runoff was described as occurring primarily over the fraction of a grid square where the soil had become saturated due to a high water table or impermeable surface soil. The transpiring surface was specified by seasonal changes in leaf area index (Dickinson et al. 1993). In RegCM4, new land-use types were added to BATS to represent urban and suburban environments (Giorgi et al. 2012). This kind of urban land use has little impact on TP climate simulation due to the sparse population.

CLM3.5 (Oleson et al. 2007) is an improvement and development of CLM3. New surface datasets and parameterizations were implemented in CLM3. The modifications consist of surface datasets based on the

Table 1. The model structure of Biosphere-Atmosphere Transfer Scheme (BATS) and Community Land Model version 3.5 (CLM3.5) land surface schemes. GLCC: global land cover characterization; MODIS: Moderate Resolution Imaging Spectroradiometer

	BATS	CLM3.5
Vertical stratification	3 soil layers, a snow layer, a vegetation layer	10 soil layers, 5 snow layers, a vegetation layer
Land cover	20 (GLCC)	5 landunits, plant functional types (PFTs) represent vegetation
Sub-grid	Each grid cell has a landunit	Each grid cell has a different number of landunits
Temperature solver	Deardoff force-restore	Heat conduction equation
Runoff	Occurring when the soil has become saturated	A simple TOPMODEL-based model
Surface datasets	Leaf area index	Multi-year MODIS products
Soil freezing and thawing	Soil freezes uniformly between 0 and –4°C, and soil thermal diffusivity is limited to 1.4×10^{-6} m^2 s^{-1}	A new frozen soil scheme (supercooled soil water)

multi-year Moderate Resolution Imaging Spectroradiometer (MODIS) products (Lawrence & Chase 2007), a simple TOPMODEL-based model (SIMTOP) for surface and sub-surface runoff (Niu et al. 2005), and a new frozen soil model (Niu & Yang 2006). Spatial land-surface heterogeneity in CLM was represented as a nested subgrid hierarchy in which grid cells were composed of multiple land units (glaciers, wetlands, lakes, urban area, and vegetated land cover), snow/soil columns, and plant functional types. The model included a 10-layer soil column, a 5-layer snow module, and a 1-layer vegetation model. The heat-conduction equation was solved numerically to calculate soil and snow temperatures (Oleson et al. 2004).

2.2. Experimental design and data

The regional climate models used in the present work were RegCM3 and RegCM4.3.4. The RegCM3 regional climate model was updated and developed based on a second-generation RegCM by the Abdus Salam International Center for Theoretical Physics (Giorgi et al. 1993a, 1993b, Pal et al. 2007). These improvements involved a representation of the CCM3 radiative-transfer scheme (Kiehl et al. 1996), an updated land-surface scheme (BATS 1e) (Dickinson et al. 1993), a large-scale cloud and precipitation scheme (Pal et al. 2000), new parameterizations of ocean surface fluxes (Zeng et al. 1998), and a cumulus convection scheme (Emanuel 1991, Emanuel & Živkovic-Rothman 1999). RegCM4 represents a substantial evolution of its previous version, RegCM3 (Pal et al. 2007). Several physical processes in the model, including new land-surface, planetary boundary layer, and air–sea flux schemes, a mixed convection and tropical band configuration, and modifications to the existing radiative-transfer model, have been continuously updated since the previous version. On the whole, the performance of RegCM4 shows some improvement in several respects (Giorgi et al. 2012). The major addition to RegCM4 is the option of using a more advanced land-surface process model, CLM3.5, which is described in detail by Oleson et al. (2004, 2008). BATS has also been added as an alternative land-surface scheme.

We performed 3 sensitivity studies of the impact of surface–atmosphere coupling on regional climate model simulation over the TP (Table 2): (1) RegCM3 coupled with BATS (RegCM3_BATS); (2) RegCM4 coupled with BATS (RegCM4_BATS); and (3) RegCM4 coupled with CLM3.5 (RegCM4_CLM). The same simulation domain covering the TP and adjacent regions was designed for the 3 experiments (Fig. 1). In these simulations, the center point of the 3 experiments was set as 30° N, 90° E. The horizontal grid consisted of 108 and 160 points in the latitudinal and longitudinal directions respectively, with 30 km resolution, and 23 vertical layers with the model top at 10 hPa. Twelve grid points in each direction were allocated for each lateral buffer zone. Six hourly fields from European Centre for Medium Range Weather Forecast 40 yr reanalysis (ERA40) data were used to provide the initial conditions and lateral boundary forcing for the regional model in all experiments. Sea-surface temperatures (SSTs) were acquired from NOAA optimal interpolation weekly SST data (1 × 1° resolution). An integration time step of 60 s was used. The Grell cumulus cloud convective parameterization scheme was used with the FC80 closure assumption (Grell 1993, Yang & Yang 2008).

Table 2. Configuration of models applied to analyze the influence of different land-surface schemes (BATS and CLM; see Table 1) on regional climate models. ICBC: Initial and boundary conditions; ERA40: European Centre for Medium Range Weather Forecast 40 yr reanalysis

Physics	RegCM3_BATS	RegCM4_BATS	RegCM4_CLM
Regional climate model	RegCM3	RegCM4.3.4	RegCM4.3.4
ICBC	ERA40, relaxation (exponential)	ERA40, relaxation (exponential)	ERA40, relaxation (exponential)
Simulation period	Nov 1, 1991–Feb 1, 2002	Nov 1, 1991–Feb 1, 2002	Nov 1, 1989–Feb 1, 2002
Analysis period	1992–2001	1992–2001	1992–2001
Vertical layers (top)	23 layers (10 hPa)	23 layers (10 hPa)	23 layers (10 hPa)
Horizontal resolution	30 km	30 km	30 km
Horizontal grid number	108 × 160	108 × 160	108 × 160
Cumulus convection	Grell with Frisch-Chappell	Grell with Frisch-Chappell	Grell with Frisch-Chappell
Land surface	BATS	BATS	CLM3.5

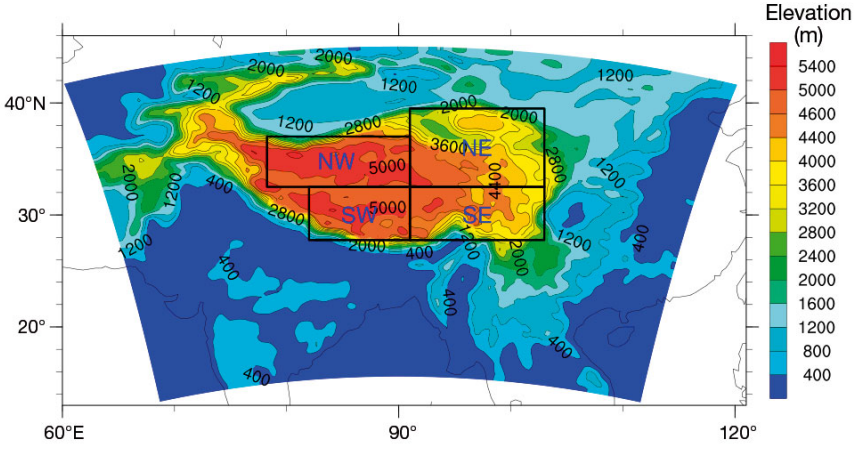

Fig. 1. Model domain and topography (m) of the study region on the Tibetan Plateau. The solid boxes represent the 4 sub-regions: NW, NE, SW, and SE

The simulation periods of the experiments were November 1, 1991 to February 1, 2002 for RegCM3_BATS and RegCM4_BATS, and November, 1 1989 to February 1, 2002 for RegCM4_CLM. The period from January 1, 1992 to December 31, 2001 (10 yr) was considered in the analysis. The months before 1992 were discarded as initialization time. The 0.5° gridded daily observation temperature (CN05) (Xu et al. 2009) and 0.25° gridded daily observation precipitation (CN05.1) (Wu & Gao 2013) (hereafter referred to collectively as CN05) were used to evaluate regional-scale features of simulated temperature and precipitation.

To examine the simulated results in more depth, the TP was divided into 4 sub-regions (Fig. 1): NW (32.5 to 37° N, 78.25 to 91° E), SW (27.75 to 32.5° N, 82 to 91° E), SE (27.75 to 32.5° N, 91 to 103° E), and NE (32.5 to 39.5° N, 91 to 103° E). Wang (2006) considered that 32 to 33° N was the boundary between the northern and southern TP because of differences in the variation of warm-season air temperatures on a decadal time scale. 32.5° N was therefore defined as the dividing line between the south and north. The area around 91° E is the mountainous area of the plateau and is also the western boundary of the Qaidam Basin. The 4 sub-regions basically covered the plateau areas above 3000 m elevation (Qu et al. 2009). The CN05 daily precipitation and temperature data, which are widely used in climate validation research, were used to validate simulated temperature and precipitation for the 4 sub-regions. In addition, in this research, spring was assumed to include March, April and May; summer to include June, July, and August; autumn to include September, October, and November; and winter to include December, January, and February.

3. RESULTS AND DISCUSSION

3.1. Temperature

The TP 10 yr (1992–2001) average temperature distributions from the 3 simulation models (RegCM3_BATS, RegCM4_BATS, and RegCM4_CLM) using the CN05 data set are shown in Fig. 2. The 3 models showed good performance in simulating the spatial distribution of temperature over the TP. The major spatial patterns show consistency with the topography, i.e. it is warm in low-terrain regions and cold in high-terrain regions. This result is also in agreement with those of Wang et al. (2013). The simulated temperatures are lower than the CN05 data

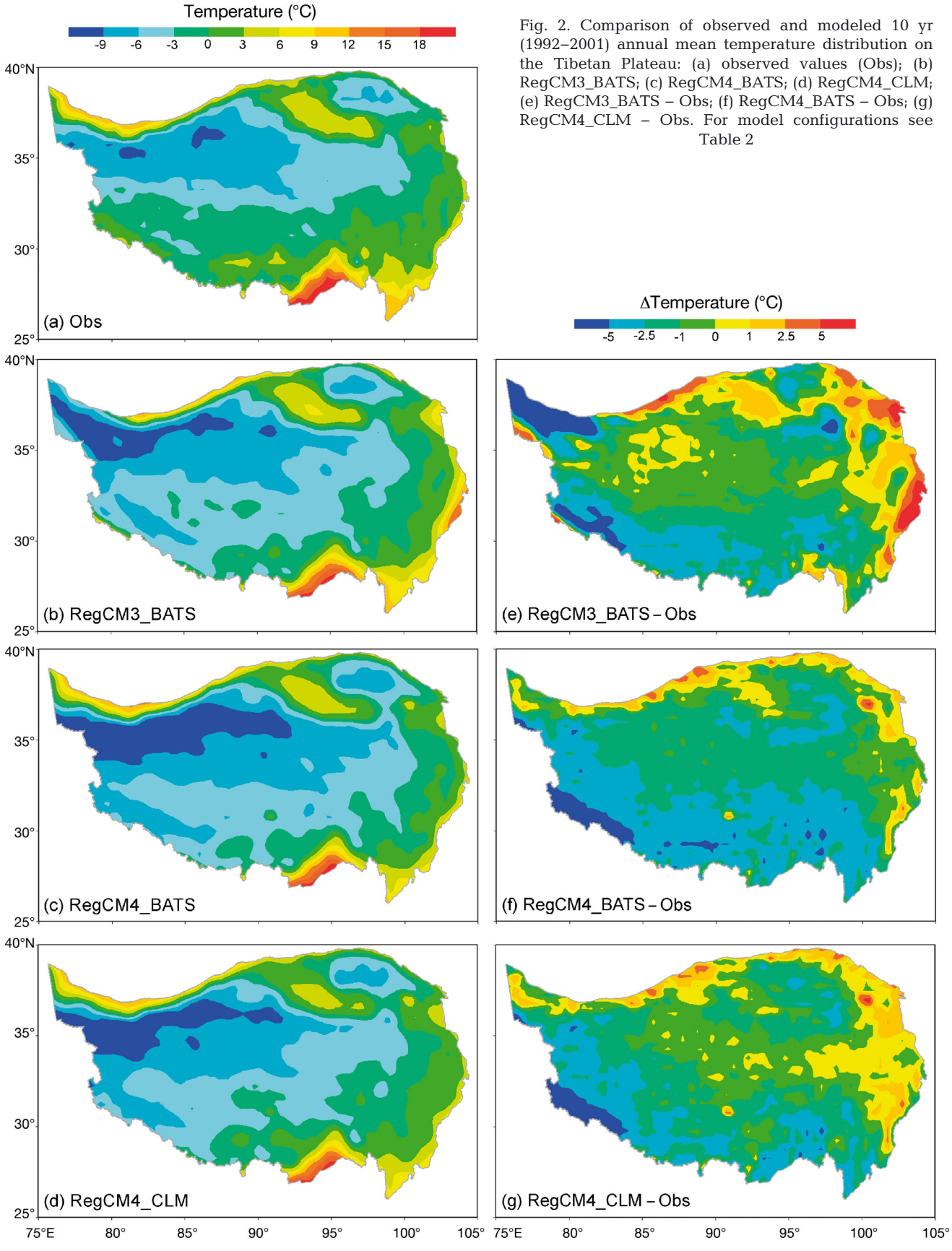

Fig. 2. Comparison of observed and modeled 10 yr (1992–2001) annual mean temperature distribution on the Tibetan Plateau: (a) observed values (Obs); (b) RegCM3_BATS; (c) RegCM4_BATS; (d) RegCM4_CLM; (e) RegCM3_BATS – Obs; (f) RegCM4_BATS – Obs; (g) RegCM4_CLM – Obs. For model configurations see Table 2

(Fig. 2a–d), a phenomenon which may be related to biases in the reanalysis forcing data (Ma et al. 2008, Wang & Zeng 2012). For the whole TP, the averaged simulation results from RegCM3_BATS were 1.22°C lower than those from CN05 (Fig. 2e). There were major cold biases in the western Kunlun Mountains and the western Himalayan Mountains, but warm biases in the Qilian and Hengduan Mountains in RegCM3_BATS compared with CN05. The regional average simulation results from RegCM4_BATS were 2.11°C lower than those from CN05. As for RegCM4_BATS, the large cold biases in the Himalayan and Hengduan Mountains were clearly evident, but warm biases similar to those in RegCM4_BATS still existed (Fig. 2f). However, the areas of substantial cold and warm bias in the CLM scheme were not as large as in the BATS scheme, which means that the cold and warm biases were significantly reduced in the CLM scheme compared to the BATS scheme. The regional average simulation results from RegCM4_CLM were 1.32°C lower than those from CN05 (Fig. 2g).

Taylor diagrams (Taylor 2001) derived from the correlation coefficients and standard deviations of the simulated results and the observations provide a way to summarize graphically how closely a pattern (or a set of patterns) matches a set of observations. As shown in Fig. 3a, the simulation capabilities of the various land-surface schemes over the TP were not uniform. The standard deviation of the BATS scheme was lower than that of CN05 except in spring. Compared with the other 2 models, RegCM4_CLM best matched the observed annual mean and seasonal temperatures, with relatively high correlations and small root mean square errors. The correlation coefficients all exceed 0.90 (99% confidence level) and the simulated results for spring and winter were in relatively good agreement with CN05. After dividing the TP into 4 sub-regions and comparing the results with

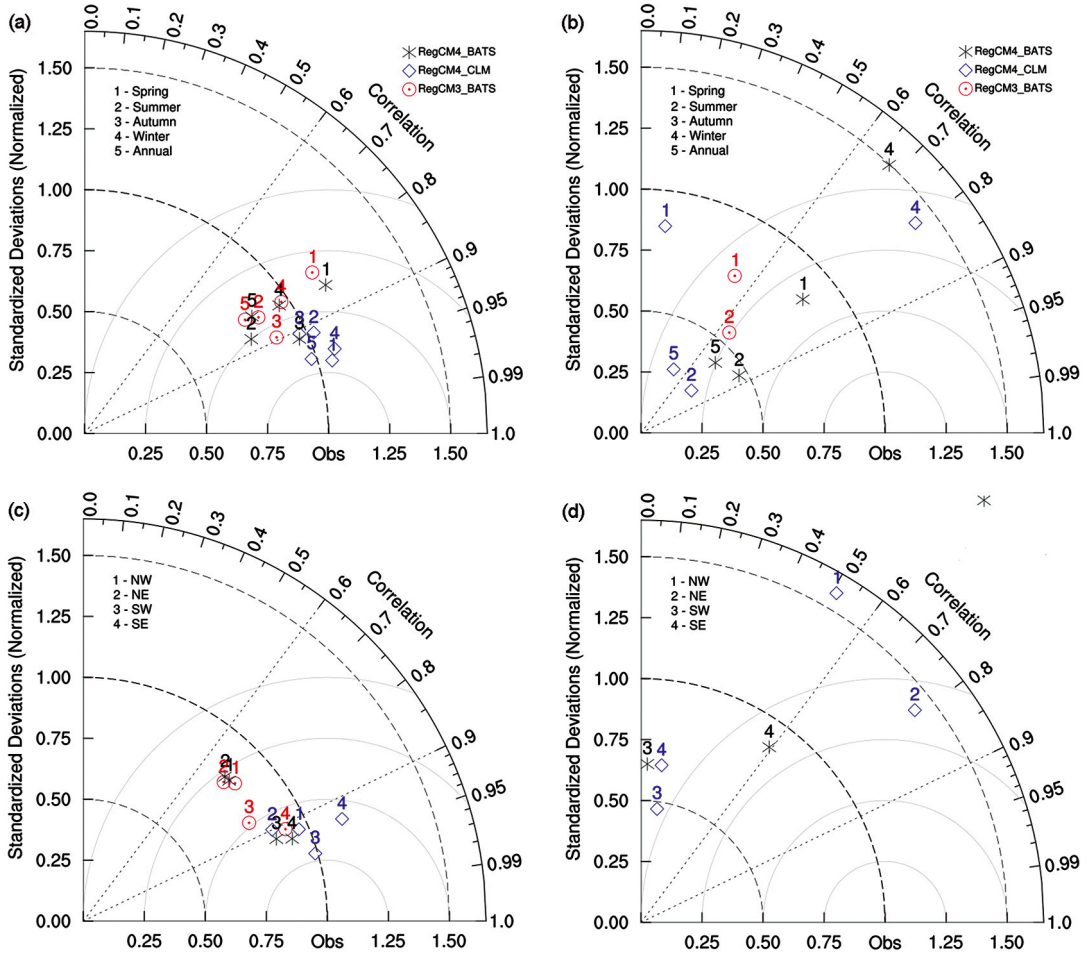

Fig. 3. Taylor diagram of 10 yr average simulation capabilities of 3 RegCM simulation over the Tibetan Plateau (TP) according to observed data for (a) seasonal temperature; (b) seasonal precipitation; (c) sub-regional temperature ; (d) sub-regional precipitation. For model configurations see Table 2

CN05 data, the correlation coefficients between simulated results and observations were within the 0.70 to 0.96 range and exceeded the 95% confidence level (Fig. 3c). The simulated temperatures were all lower than the observed data, especially in the NE, with small biases. The standard deviations in most regions (except for the SE in RegCM4_CLM) were lower than the observed values. The 3 models performed better in the SW and SE, as indicated by relatively high correlations and small root mean square errors. Reg CM4_CLM generally agreed best with CN05 in all 4 sub-regions.

3.2. Precipitation

In general, precipitation is relatively difficult to simulate in a climate model. This is particularly true in the TP, where precipitation shows considerable spatio-temporal variations. In this respect, this region poses one of the most challenging problems for climate simulation. Fig. 4 shows that the main features of the rainfall belts captured by the 3 models agree with the CN05 observations. Broadly speaking, precipitation decreases from south to north along the latitudinal gradient. The area with least rain is the Qaidam Basin, with an average annual precipitation of 150 mm (Fig. 4a). Although the observed precipitation patterns were well reproduced (Fig. 4c,d), all 3 models overestimated the TP average annual precipitation amounts (with errors up to 271.81 mm or 43.2% for RegCM3_BATS, 354.49 mm or 49.8% for RegCM4_BATS, and 80.44 mm or 18.4% for RegCM4_CLM). Compared with the CN05 data, the models consistently underestimated precipitation in the Qaidam Basin, the Qiangtang Plateau, and the middle section of the Himalaya Mountains, whereas they overestimated precipitation in the rest of the TP (Fig. 4e–g). In addition, with the exception of the Qaidam Basin and the western Qiangtang Plateau, the precipitation amounts from RegCM4_CLM appeared to be generally smaller in the southern and southeastern TP than those from the BATS scheme. Notable improvements in simulated precipitation in RegCM4_CLM included the reduction of precipitation overestimation in the BATS scheme in the northern and northeastern parts of the plateau (Fig. 4g).

The Taylor diagram (Fig. 3b) shows that the correlation coefficients of annual and seasonal precipitation were generally smaller than those of annual and seasonal mean temperature, while the ratios of standard deviation were further from unity than those for annual and seasonal mean temperature. This indicates that annual and seasonal mean temperatures were better estimated than annual and seasonal precipitations. The annual and seasonal standard deviations as simulated by RegCM4_CLM were lower (except in winter) than observed values. However, Reg CM4_BATS yielded slightly higher correlations in summer (0.86) than the other models. The simulated summer precipitation was relatively consistent with the CN05 data compared to other seasons. However, the simulated autumn precipitation values from the 3 models were all negatively related to the CN05 data, a phenomenon which is not shown in Fig.3b. Among the 3 models, RegCM4_CLM best represented the observed mean annual precipitation, as shown by a high correlation and a small mean error. The simulated standard deviations of RegCM3_BATS were much larger than the CN05 data. In the SE region, the simulated standard deviation of RegCM4_BATS was much closer to the CN05 data (Fig. 3d). However, it was notable that precipitation simulated by RegCM4_CLM was less well matched to observed value in the SE region. This leads to conclusions similar to those illustrated in Fig. 4g, for reasons which will be further discussed in Section 3.5.

3.3. Surface water balance

3.3.1. Surface soil moisture

In the BATS scheme, 3 parameters, surface soil water (representing water in the upper soil layer), water at the soil root-zone depth, and total water in the soil to depth were considered to represent soil moisture (Dickinson et al. 1993). In CLM3.5, soil wetness is defined as the ratio of volumetric liquid water content to the difference of saturated water content minus volumetric ice content (Oleson et al. 2007). Fig. 5 shows annual mean, summer, and winter surface soil moisture at 10 cm depth, as simulated by the 3 models. The spatial distributions of soil moisture simulated by the 3 models generally matched those for precipitation. Relatively speaking, surface soil moisture over the TP was highest according to RegCM4_BATS, followed by RegCM3_BATS and then RegCM4_CLM. This was particularly evident in summer. As the rainy season approached, surface soil moisture increased. Large differences in simulated precipitation probably caused consequential differences in soil moisture. In winter, most surfaces started to freeze when the temperature was <0°C. Surface soil moisture declined sharply, especially in the north-central TP (<5 kg m^{-2}). In most parts of the plateau, soil moisture

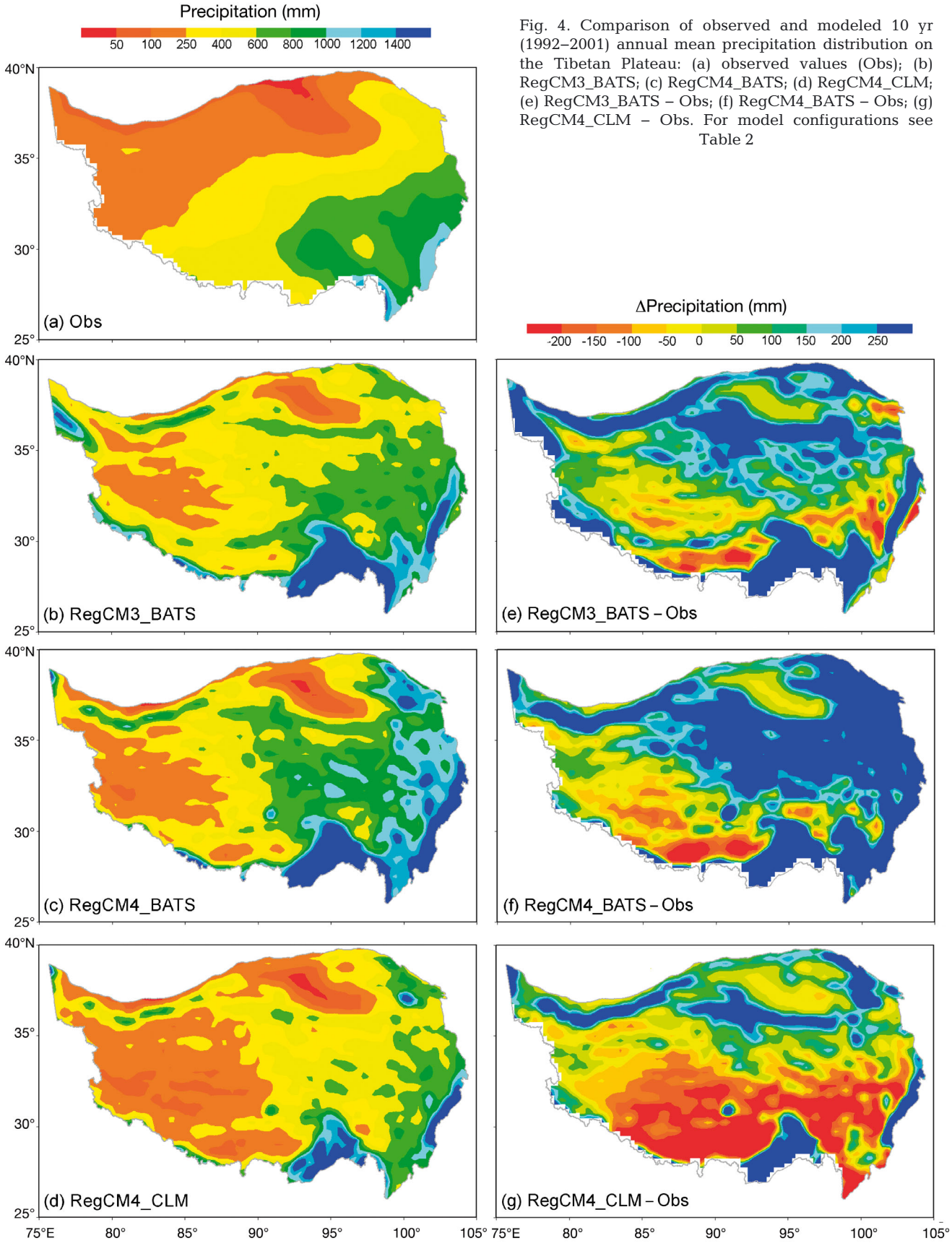

Fig. 4. Comparison of observed and modeled 10 yr (1992–2001) annual mean precipitation distribution on the Tibetan Plateau: (a) observed values (Obs); (b) RegCM3_BATS; (c) RegCM4_BATS; (d) RegCM4_CLM; (e) RegCM3_BATS – Obs; (f) RegCM4_BATS – Obs; (g) RegCM4_CLM – Obs. For model configurations see Table 2

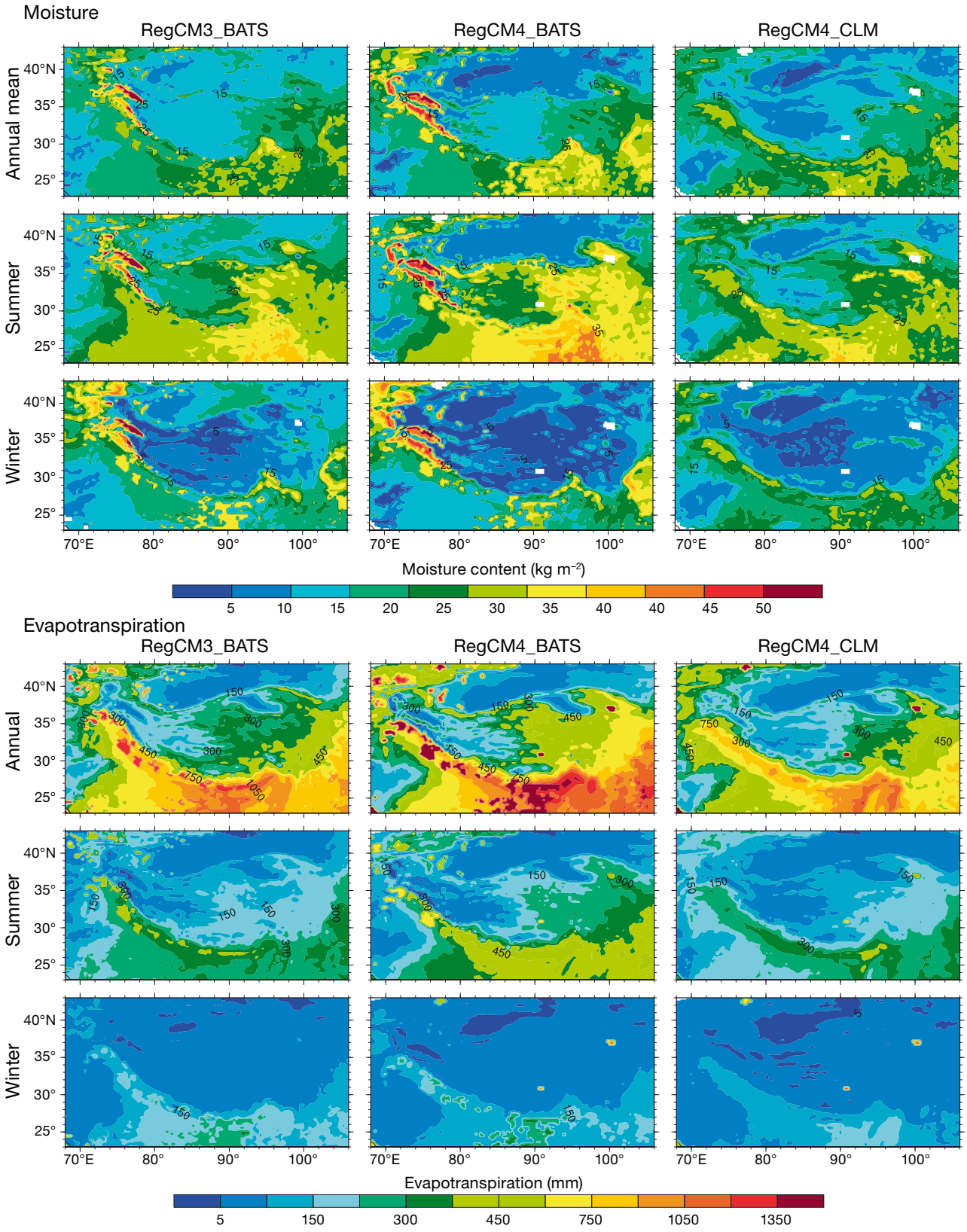

Fig. 5. Annual and seasonal 10 cm soil moisture content and evapotranspiration on the Tibetan Plateau over the 10 yr simulation time period (1992–2001) for the models RegCM3_BATS, RegCM4_BATS and RegCM4_CLM

in RegCM4_BATS was relatively low. This occurred in part because of significant differences in the treatment frozen soil between the 2 land-surface schemes. The concept of supercooled soil water, which is liquid water that coexists with ice over a wide range of temperatures below freezing, was introduced into CLM3.5 (Niu & Yang 2006), but is not included in soil water content in BATS.

3.3.2. Evapotranspiration

In the BATS model, the current expressions for evaporation are based on the behavior of a soil column that is initially at field capacity and then is dried by a diurnally varying potential evaporation factor applied at the surface (Dickinson et al. 1993). However, soil evaporation in CLM3.5 depends on the specific humidity values of the soil surface and the canopy air and the aerodynamic resistance to water-vapor transfer between the ground and the canopy air (Oleson et al. 2007). The 3 models all exhibited similar spatial patterns of annual, summer, and winter evapotranspiration (ET). High-ET areas, with annual values up to a maximum of 1050 mm, occurred in the Karakoram and Himalaya mountains and in the southern TP (Hengduan Mountains). Annual ET in these areas varied up to a maximum of 1050 mm. ET values were 300 to 450 mm in the eastern plateau, and <150 mm in the Qiangtang Plateau and the Qaidam Basin (Fig. 5). ET was greater in RegCM4_BATS than in the other two models. This result was similar to that found by Steiner et al. (2009).

In summary, soil moisture values, especially in summer, as simulated by RegCM4_CLM were lower than those simulated by RegCM3_BATS and Reg CM4_BATS, resulting in lower local ET (Fig. 5) and thereby probably causing local precipitation to decrease (Fig. 4). Decreased precipitation then contributed to further soil drying. This positive feedback effect, from soil moisture to precipitation and ET, which was summarized by Seneviratne et al. (2010), could potentially lead to a continued further decrease in soil moisture, until precipitation occurs as a result of large-scale circulation.

The highest 10 yr average ET values for the 4 sub-regions (NW, NE, SW, and SE) were simulated by RegCM4_BATS (Table 3). With reference to particular regions, the largest annual ET (671.15 mm) was in the SE, where soil moisture was also highest. The sub-regional ratios of annual ET to annual precipitation (ET:Pre) (Yang et al. 2007b, Steiner et al. 2009) were largest in RegCM4_CLM, except for in the NW. Values of ET:Pre for the whole TP region during the corresponding period in RegCM3_BATS, RegCM4_BATS, and RegCM4_CLM were 47.6, 62.9, and 65.2% respectively. With respect to seasonal variations, the largest summer and autumn ET:Pre values for the NE, SW, and SE regions were in RegCM4_CLM (Fig. S1 in the Supplement at www.int-res.com/articles/suppl/c062p025_supp.pdf). In summer, ET represented approximately 50.3, 56.9, and 60.6% of precipitation in RegCM3_BATS, RegCM4_BATS, and RegCM4_CLM respectively. The ET:Pre ratio in RegCM4_CLM was much closer to the results presented by Yang et al. (2007b) for the northern TP.

Table 3. Ten yr (1992–2001) average surface energy and water balances simulated for 4 sub-regions (NW, NE, SW and SE) of the Tibetan Plateau by 3 regional climate models (RegCM3_BATS, RegCM4_BATS, and RegCM4_CLM; see Table 2). Pre: precipitation; ET: evapotranspiration; RO: runoff; ISR: incoming solar radiation; NSR: net shortwave radiation; NLR: net longwave radiation; SHF: sensible heat flux; LHF: latent heat flux

		Water balance (mm)				Energy terms (W m^{-2})				
		Pre	ET	RO	Storage	ISR	NSR	NLR	SHF	LHF
NW	RegCM3_BATS	403.90	233.31	3.64	166.95	177.37	118.09	67.10	32.33	19.86
	RegCM4_BATS	390.87	292.09	3.33	95.45	233.87	161.76	93.58	45.08	24.98
	RegCM4_CLM	246.64	146.05	8.79	91.81	242.00	162.17	104.68	47.41	12.37
NE	RegCM3_BATS	581.76	293.30	7.58	280.88	153.99	112.04	61.47	25.49	24.45
	RegCM4_BATS	708.41	457.23	11.21	239.98	201.07	158.13	85.50	35.99	38.16
	RegCM4_CLM	430.87	292.40	8.18	130.29	216.85	175.38	99.10	37.80	24.31
SW	RegCM3_BATS	575.70	332.39	5.76	237.55	199.80	149.55	79.67	45.50	27.35
	RegCM4_BATS	492.98	385.42	4.85	102.72	256.58	200.89	105.59	68.42	31.84
	RegCM4_CLM	296.64	258.16	5.15	33.33	264.02	206.30	118.82	61.40	21.34
SE	RegCM3_BATS	1208.67	460.56	24.85	723.26	169.42	126.60	59.64	28.55	37.73
	RegCM4_BATS	1278.05	671.15	26.97	579.94	215.25	181.65	79.20	46.54	55.14
	RegCM4_CLM	779.32	446.93	19.70	312.70	233.37	200.53	96.16	54.52	36.65

These results suggest that due to the high ET per unit precipitation, RegCM4_CLM returned the most water vapor to the atmosphere among the 3 models.

3.3.3. Runoff and soil water storage

Surface runoff is influenced by precipitation, snow melt, underlying surface characteristics (such as soil freezing/thawing state and soil texture), and the underground water table. Surface runoff as simulated by the BATS scheme was significantly affected by precipitation (Fig. 6). With increasing (decreasing) in precipitation, surface runoff increased (decreased). Its peak followed the precipitation peak in time. In the BATS scheme, surface runoff is parameterized by saturated soil-water density, soil-water density weighted toward the top layer, and surface temperature (Dickinson et al. 1993). These surface parameters relate to 12 specific soil texture classes, ranging from 1 = very coarse (equivalent to sand) to 12 = very fine (equivalent to heavy clay). However, the annual cycle of surface runoff in the CLM scheme is quite different. Surface runoff in most regions showed a peak around April, partly because low soil permeability induced by the excessive surface-soil ice content enhanced surface runoff in spring (Niu & Yang 2006). In addition, unfrozen water content and snow melt increased because the ground temperature was rising at this time (Fig. S2 in the Supplement at www.int-res.com/articles/suppl/c062p025_supp.pdf), which directly contributed to surface runoff. This agreed with the results obtained by Wang et al. (2009). The annual cyclic pattern of simulated runoff in the CLM scheme was also in line with the results of Zeng et al. (2002) for western Siberia. Later on, summer runoff decreased gradually, mainly because ice content diminished with rising temperatures, with a corresponding increase in the fractional permeable area, resulting in lower runoff (Zhou et al. 2000, Niu & Yang 2006). The runoff coefficient in RegCM3_BATS was roughly congruous with that in RegCM4_BATS. However, the CLM scheme had a relatively higher runoff coefficient over the TP than the BATS scheme, except in summer (Fig. S1).

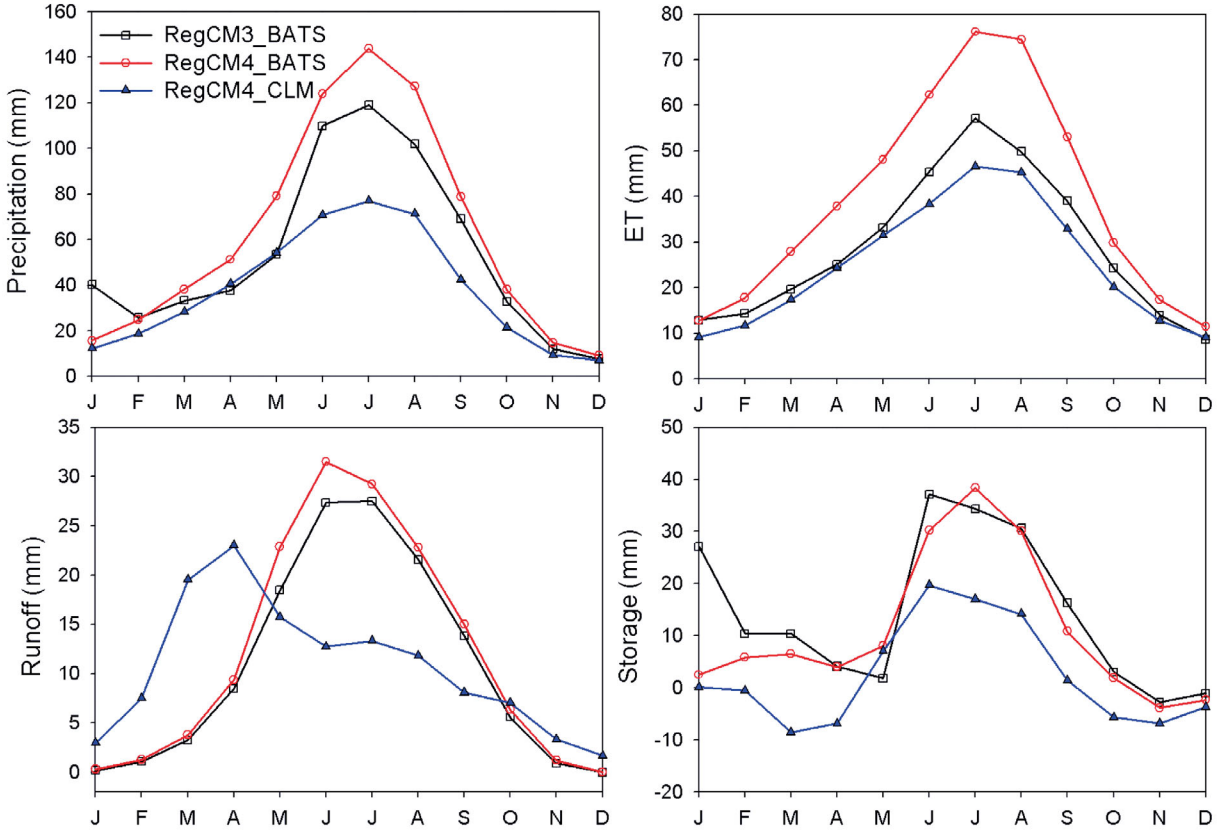

Fig. 6. Average monthly water balance items on the Tibetan Plateau over the 10 yr simulation time period (1992–2001) for the models RegCM3_BATS, RegCM4_BATS, and RegCM4_CLM. ET: evapotranspiration

Higher precipitation values in the BATS scheme tended to cause more water to be stored in the soil layers. This phenomenon was consistently manifested in every sub-region and for most seasons (Table 3 & Fig. 6). Similarly, the partitioning of precipitation to soil-water storage was also larger in the BATS scheme (Fig. S1). The partitioning of precipitation to water storage decreased proportionally as the partitioning of precipitation to ET increased.

3.4. Surface energy budget

3.4.1. Radiation balance

Although the annual cycles of incoming solar radiation (ISR) were broadly uniform, the month of occurrence of the maximum was different in the 3 models (Fig. 7). The month of maximum ISR in RegCM4_BATS and RegCM4_CLM was May, whereas in Reg CM3_BATS, it occurred in June (NW and SW) or in July (NE and SE). Seasonal variations in ISR were mainly affected by movement of the solar vertical incidence point, precipitation, and cloud cover. As the solar vertical incidence point moved across the Equator to the Tropic of Cancer, ISR gradually increased. It reached its maximum before the onset of the plateau summer monsoon (about the end of May to the middle of June). ISR then decreased as summer precipitation and cloud-cover increased. ISR values in the CLM scheme were higher than in the BATS scheme in most sub-regions and seasons (except for January in the SW and SE). These biases, especially in summer and autumn, were largely attributable to underestimation of precipitation by the CLM scheme (Figs. 4 & 6). Moreover, annual mean ISR over the TP was also higher in the CLM scheme than in the BATS scheme (Table 3), leading to higher temperatures in the CLM scheme than in the BATS scheme (Fig. 3a).

Net shortwave radiation (NSR) is the ISR after surface reflection. Therefore, its magnitude depends on the ISR and on surface albedo. The annual cycles of NSR are similar to those of ISR, with highest values, on average, in RegCM4_CLM. Fig. 8 shows the longitude-month cross section of zonal albedo and the latitude-month cross section of meridional albedo during 1992–2001. Surface albedo on the TP, which is influenced by surface snow cover and soil moisture, varied with the seasons. However, coherent spatial and temporal distribution patterns were reproduced by the 2 land-surface schemes. Albedo values were higher in the west than in the east, and higher in winter than in summer. As mentioned above, RegCM3_BATS significantly underestimated the temperature of the Kunlun and western Himalayan Mountains, where more precipitation occurred than predicted by RegCM4_CLM (Fig. 4e). Therefore, it can be speculated that overestimated precipitation in these areas caused larger snow-cover areas (corresponding to higher snow albedo in Fig. 8), leading to more solar-radiation reflection during the daytime, which in turn led to lower air temperature. A similar speculation can be found in Jin et al. (2010). However, the cold bias of the Kunlun Mountains was not seen in RegCM4_CLM, indicating that detailed descriptions of land-surface processes in the CLM scheme played a role in this improvement. Albedo as simulated by RegCM4_CLM between 26° and 40° N was obviously smaller because of drier soil conditions (Fig. 5), which made it more difficult for soil to absorb solar radiation, resulting in higher NSR. This was consistent with the results for the NE and SE shown in Fig. 7. Between 70° and 90° E, RegCM4_CLM simulated higher albedo in winter and spring, but lower albedo in summer and autumn compared to Reg CM4_BATS, resulting in lower NSR in the NW and SW in spring and winter, but only slightly higher values in summer.

Net longwave radiation (NLR) is the balance between surface upward longwave radiation and atmospheric downward longwave radiation. NLR in the CLM scheme is higher than in BATS. Differences in NLR among the 3 models increased at the onset of the rainy season because more precipitation was simulated by the BATS scheme, especially by RegCM4_BATS (Fig. 4). At the start of the rainy season, cloud cover and abundant water vapor created more downward longwave radiation, whereas upward longwave radiation from the surface decreased, generating lower NLR in the BATS scheme, for example in the SE and SW.

Because of the higher NSR and NLR values simulated by the CLM scheme, net radiation (NSR + NLR) in CLM was also higher. The NSR values simulated by RegCM4_CLM were close to those from Reg CM4_BATS in the NW and SW, and therefore no significant differences were found between the 2 models.

3.4.2. Sensible and latent heat flux

Sensible heat fluxes (SHF) as simulated by RegCM4_CLM were obviously higher in most seasons (winter and spring) and most sub-regions (NW,

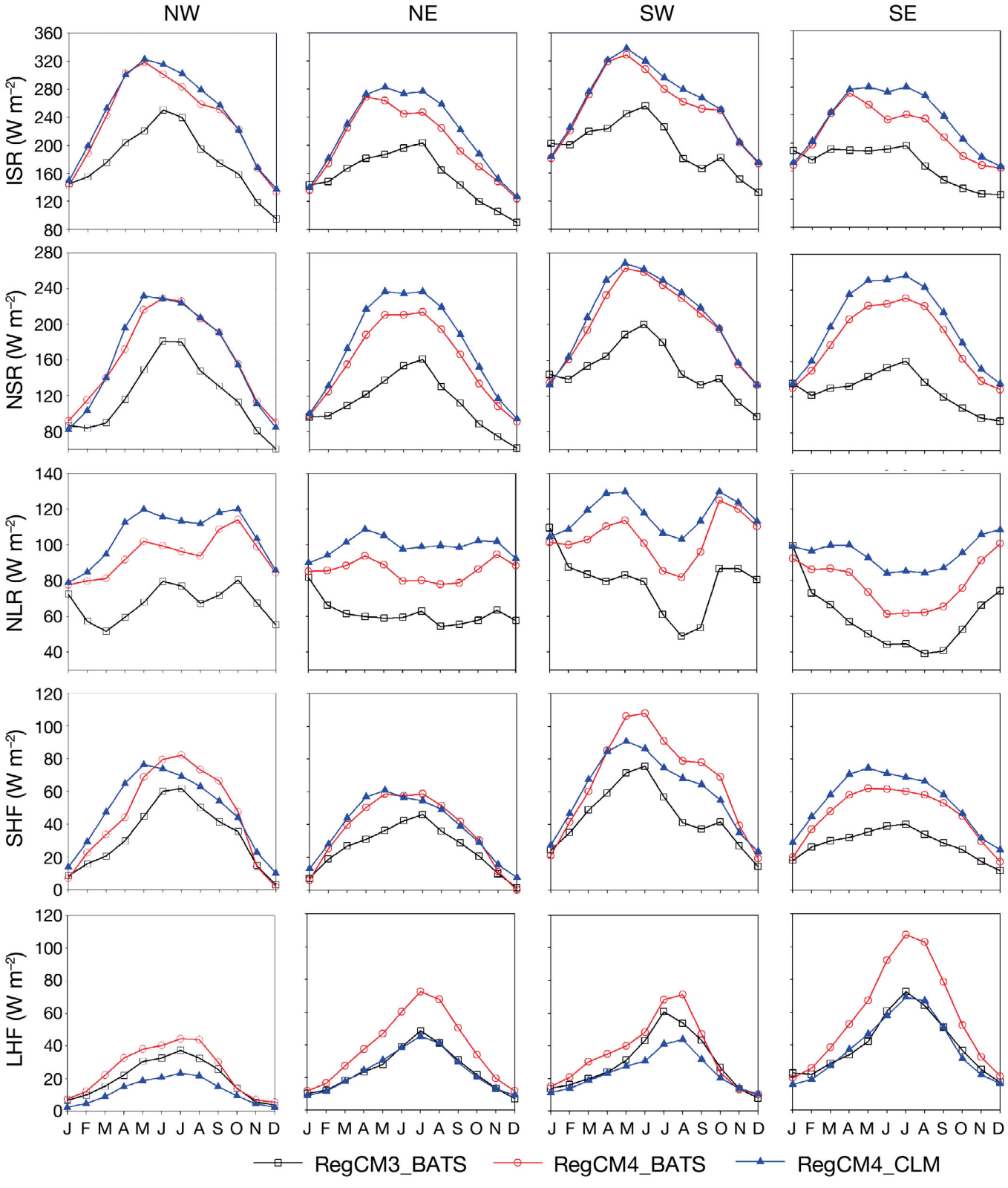

Fig. 7. Average monthly water balance items in the 4 sub-regions (NW, NE, SW and SE) of the Tibetan Plateau over the 10 yr simulation time period (1992–2001) for the models RegCM3_BATS, RegCM4_BATS, and RegCM4_CLM. ISR: incoming solar radiation; NSR: net shortwave radiation; NLR: net longwave radiation; SHF: sensible heat flux; LHF: latent heat flux

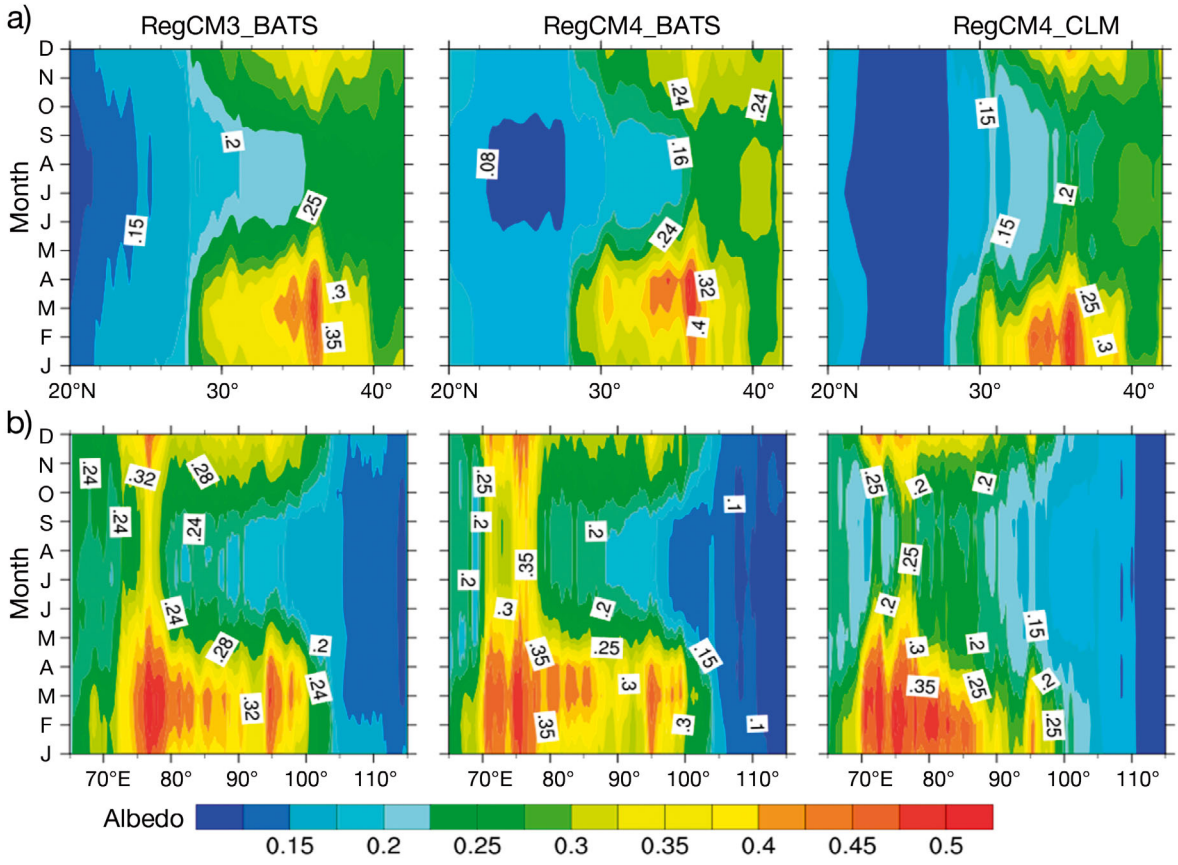

Fig. 8. Average (a) latitude-month (averaged between 78.25° and 103° E) and (b) longitude-month (averaged between 27.75° and 39.5° N) albedo profiles on the Tibetan Plateau over the 10 yr simulation time period (1992–2001) for the models RegCM3_BATS, RegCM4_BATS and RegCM4_CLM

NE, SW) than those from the other models. In the SE, the CLM scheme produced higher SHF throughout the year than BATS. Overall, The SHF values from RegCM3_BATS were the lowest over the TP. In the NW, NE, and SE, average SHF values were largest in RegCM4_CLM. However, the highest SHF in the SW was simulated by RegCM4_BATS. SHF simulated by RegCM4_CLM was 1.28 and 17.32 W m^{-2} higher than in RegCM4_BATS and RegCM3_BATS, respectively, over all sub-regions (Table 3). Seneviratne et al. (2010) asserted that decreased ET leads to an increase in SHF and therefore an increase in air temperature. This would explain why the air temperature in RegCM4_CLM was higher than that in Reg CM4_BATS (Fig. 2c,d).

Latent heat flux (LHF) is related to the latent heat of fusion of snow cover and the latent heat of vaporization. The partitioning of net radiation into LHF was significantly different between the BATS and CLM scheme. This occurs because the LHF, along with runoff, is constrained by precipitation, which differed greatly among the 3 models. The LHF produced by RegCM4_BATS was highest throughout the whole year except in October and November in the SE (Fig. 7) and for the 10 yr average (Table 3). This was related to positive biases in precipitation (Fig. 6), surface soil moisture, and ET (Fig. 6) in the RegCM4_BATS simulations. The 10 yr average LHF simulated by RegCM4_CLM was 13.86 and 3.68 W m^{-2} lower than in RegCM4_BATS and Reg CM3_BATS, respectively.

The partitioning of net radiation was quite different between the CLM and BATS schemes, with a higher SHF, lower LHF, and hence a much higher Bowen ratio in the CLM scheme. Zeng et al. (2002) demonstrated a similar result. In summary, RegCM4_ CLM overestimated net radiation by 24.21 and 97.25 W m^{-2} and SHF by 1.28 and 17.32 W m^{-2}, but underestimated LHF by 13.86 and 3.68 W m^{-2} with respect to RegCM4_BATS and RegCM3_BATS respectively. As a result, the net radiation produced by RegCM4_CLM was not adequately transferred to the atmosphere in the form of LHF, but was stored in the surface layers, causing relatively warmer biases in air and ground temperature (Fig. S2 in the Supplement).

3.5. Wind and water-vapor mixing ratio

The spatial distributions of 10 yr winter and summer mean 500 and 200 hPa wind fields and mixing ratios are presented in Figs. 9 & 10, respectively. Compared to RegCM3_BATS, RegCM4_CLM underestimated the winter and summer water-vapor mixing ratio at 500 hPa in the TP hinterland. In winter, a cyclonic circulation appeared in the northwestern plateau as shown in Fig. 9b, indicating an anticyclonic circulation revealed by RegCM4_CLM in the northwestern plateau. This phenomenon was not predicted by RegCM3_BATS, but rather a weakened southwesterly wind, resulting in lower water vapor in the southern and southeastern plateau. In summer, the westerly wind around 40° N, the strong water-vapor convergence in the southern TP (the Indian monsoon trough), and the plateau thermal low captured by RegCM3_BATS brought moisture from the Arabian Sea and the Bay of Bengal into the southern TP and to the north of 30° N (Fig. 9d). However, RegCM4_CLM predicted very weak circulation (Fig. 9e), directly causing the lower precipitation values simulated by this model in the southern and southeastern plateau (Fig. 4). The differences in simulated mixing ratio values were much more pronounced in the lower than in the upper troposphere.

At 200 hPa, the water-vapor mixing ratio was small, and a strong westerly wind prevailed in winter (Fig. 10a). RegCM4_CLM predicted a comparatively

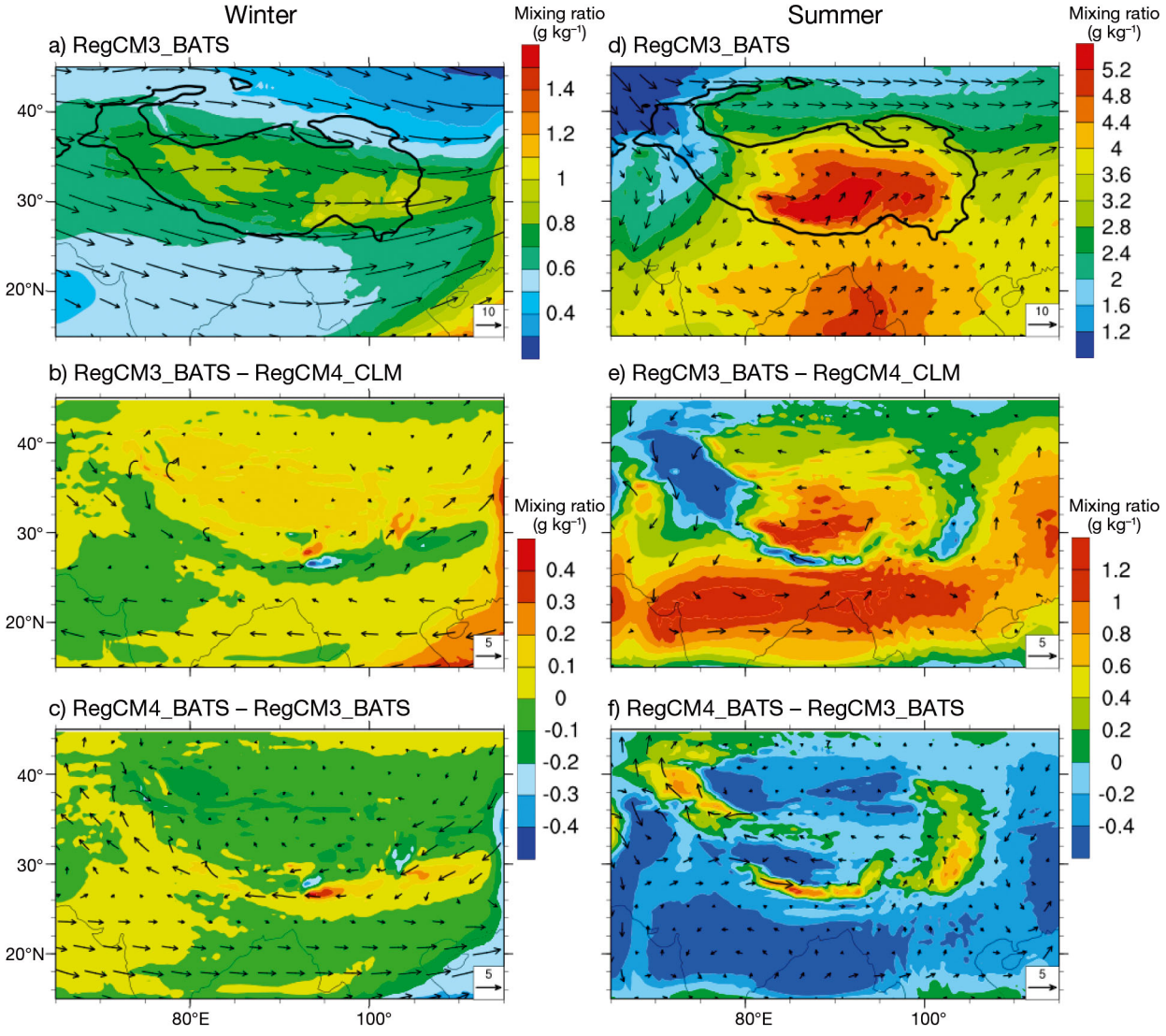

Fig. 9. Comparison of simulated spatial distribution of 10 yr winter and summer mean wind fields (m s^{-1}) and mixing ratio at 500 hPa on the Tibetan Plateau: (a,d) RegCM3_BATS; (b,e) RegCM3_BATS minus RegCM4_CLM; (c,f) RegCM4_BATS minus RegCM3_BATS. The black solid isolines in panels (a) and (d) enclose terrain above 3000 m elevation

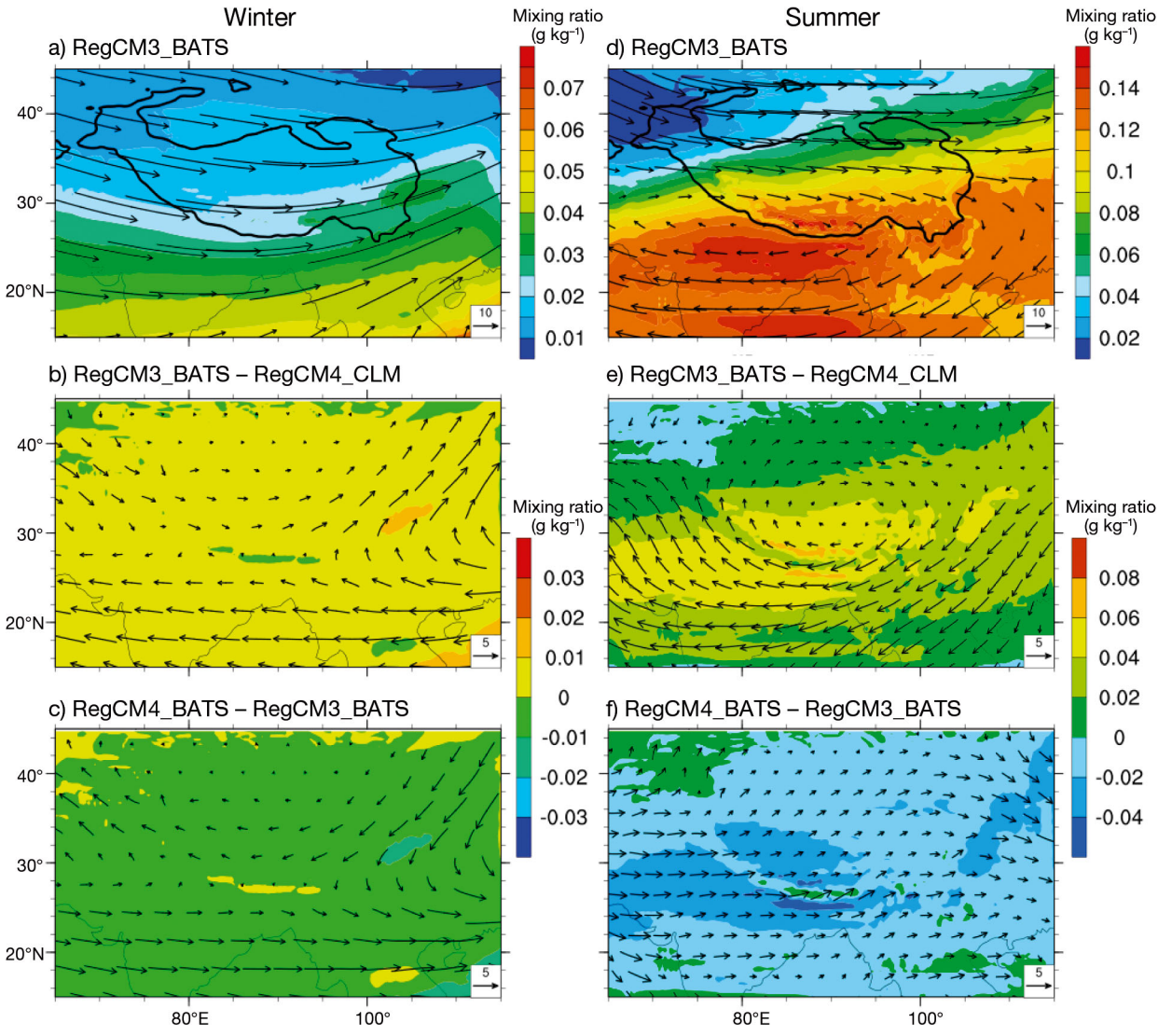

Fig. 10. Comparison of simulated spatial distribution of 10 yr winter and summer mean wind fields (m s^{-1}) and mixing ratio at 200 hPa on the Tibetan Plateau: (a,d) RegCM3_BATS; (b,e) RegCM3_BATS minus RegCM4_CLM; (c,f) RegCM4_BATS minus RegCM3_BATS. The black solid isolines in panels (a) and (d) enclose terrain above 3000 m elevation

weaker westerly wind than RegCM3_BATS, lowering the mixing ratio in the TP by 0.01 g kg^{-1} (Fig. 10b). In summer, an anticyclonic flow with horizontal divergence in the southwestern Plateau was predicted by RegCM3_BATS (Fig. 10d) along with a westerly wind in the northern to the eastern Pacific, and an easterly wind in the south to the Arabian Sea, Iran and a western area (Li 2007). In RegCM4_CLM, the northwesterly wind was weak, but the southwesterly wind was strong, resulting in persistent underestimation of the water-vapor mixing ratio (Fig. 10e). Although the mixing ratios predicted by RegCM4_BATS and Reg CM3_BATS were similar, values over the TP were consistently lower in RegCM4_BATS than in Reg CM3_BATS (Figs. 9c & 10c,f). In RegCM4_BATS, a higher mixing ratio at 500 hPa was clearly apparent in the peripheral plateau (Fig. 9f), resulting from a cyclonic flow with convergence in the western plateau and the Indian peninsula that brought moisture from the Arabian Sea and the Bay of Bengal to the northwestern, southern and eastern plateau. This is also why RegCM4_BATS simulated overall higher precipitation than RegCM3_BATS (Fig. 4).

Land surface processes are primarily driven by solar radiation, precipitation, temperature and wind. They also provide feedbacks to the atmosphere through surface energy, water, and momentum fluxes (Zeng et al. 2002). The simulated results from regional climate models are affected by ET, runoff mechanisms, and frozen soil models in land-surface

scheme as described above. Significant differences in simulated energy elements and water-balance terms exist among the 3 models, which in turn influence variations in surface temperature and moisture patterns and thereby impact atmosphere circulation and water-vapor transfer. As a result, simulated precipitation values can be underestimated or overestimated. In addition, relatively lower (higher) precipitation and drier (wetter) atmospheric conditions allow more (less) ISR to reach the surface, thereby increasing (decreasing) surface temperature. For example, precipitation was substantially reduced in RegCM4_CLM compared to the BATS scheme (Figs. 4–6). This change can be attributed mainly to land–atmosphere feedback mechanisms, because the LHF in RegCM4_CLM was much lower than in the BATS scheme (Fig. 7). Because of lower precipitation and cloud cover, NSR at the surface increased in the CLM scheme, while NLR at the surface also increased due to higher surface temperature (Figs. 7 & S2). Similar feedback mechanisms have been discussed in previous studies (Steiner et al. 2009, Diro et al. 2012). Overall, a dry bias was apparent in the CLM scheme compared to the BATS scheme; however, the ET coefficient of the CLM scheme was larger than in the BATS scheme, enhancing precipitation recycling.

4. CONCLUSIONS

This study evaluated and compared 10 yr (1992–2001) simulations on the TP by 3 regional climate models (RegCM3_BATS, RegCM4_BATS, and Reg CM4_CLM), using 2 land-surface schemes (BATS and CLM3.5), with the same domain, initial and boundary conditions (ICBC), and horizontal resolution (30 km), in order to investigate the responses of temperature and precipitation to different land-surface schemes. The major findings are summarized below.

The 3 models were all able to reproduce spatial temperature patterns. However, RegCM3_BATS, RegCM4_BATS, and RegCM4_CLM simulating 10 yr regional average temperatures showed cold biases of 1.22, 2.11, and 1.32°C, respectively, compared to CN05. High correlation coefficients between Reg CM4_CLM and CN05 indicated that RegCM4_CLM performed well in simulating annual and seasonal mean temperatures on the TP. At the sub-regional scale, all 3 models possessed good simulation capabilities in the southern and southeastern TP.

The 3 models captured well the main features of the spatial precipitation distribution. However, Reg CM3_BATS, RegCM4_BATS, and RegCM4_CLM overestimated regional average annual precipitation by 271.81 mm (43.2%), 354.49 mm (49.8%), and 80.44 mm (18.4%), respectively compared to CN05. RegCM4_CLM performed worse than the other 2 models in the southeastern plateau. With regard to seasonal effects, simulation of summer precipitation from all 3 models was better.

Surface soil moisture and ET as simulated by Reg CM4_BAT were obviously higher than in the other 2 models, whereas the smallest values occurred in RegCM4_CLM. Despite this, in terms of ET per unit precipitation, RegCM4_CLM returned more water vapor to the atmosphere, and the runoff coefficient was also relatively large. By contrast, in the BATS land-surface scheme, a higher proportion of precipitation went to soil water storage. Moreover, the CLM scheme predicted larger annual average ISR, NSR, NLR, and SHF, but smaller LHF over the TP compared to the BATS scheme, resulting in warmer temperatures.

In general, RegCM4_CLM simulates annual mean and seasonal temperatures and precipitation magnitudes over the TP better than the other 2 models. Because of the influence of the land-surface scheme used, large disparities in simulated energy elements and water-balance terms among the 3 models led to differences in surface warmth and dryness, which further affected the atmosphere, water-vapor transfer, and simulated precipitation. Furthermore, lower (higher) precipitation and a drier (wetter) atmosphere permitted more (less) shortwave radiation to warm (cool) air and surface temperatures.

In conclusion, it can be stated that TP climate simulation is extremely sensitive to different land-surface schemes in a regional climate model. Considering the deficiencies of the simulations studied here over the TP compared to observed values, further improvements to these land-surface schemes are needed. In addition, due to a lack of land-surface observations from the period before 2000, the simulated surface variables still need to be validated in future work.

Acknowledgements. This research was supported jointly by the Innovation Research Group of NSFC (41121001), the 'Strategic Priority Research Program (B)' of the Chinese Academy of Sciences (CAS) (XDB03030204), the State Key Laboratory of Cryospheric Sciences (SKLCS-ZZ-2013-02-07), CAREERI, CAS, the International Innovative Group Project of CAS (Y42AC71001), the National Natural Science Foundation of China (41075007), and the National Key Basic Research program of China (2010CB951404). We also appreciate the Supercomputing Center, CAREERI, CAS, for help with model simulations. Thanks also to Prof. Xuejie Gao for

providing the CN05 temperature data and CN05.1 precipitation data. We are grateful to the reviewers and the editor for comments on the initial draft of the manuscript.

LITERATURE CITED

Chen L, Ma ZG, Fan XG (2012) A comparative study of two land surface schemes in WRF model over eastern China. J Trop Meteorol 18:445–456

Dash SK, Shekhar MS, Singh GP (2006) Simulation of Indian summer monsoon circulation and rainfall using RegCM3. Theor Appl Climatol 86:161–172

Deardorff JW (1978) Efficient prediction of ground surface temperature and moisture with inclusion of a layer of vegetation. J Geophys Res 83:1889–1903

Dickinson RE, Henderson-Sellers A, Kennedy PJ (1993) Biosphere-Atmosphere Transfer Scheme (BATS) version le as coupled to the NCAR Community Climate Model. Technical Note NCAR/TN-387+STR, National Center For Atmospheric Research, Boulder, CO

Diro GT, Rauscher SA, Giorgi F, Tompkins AM (2012) Sensitivity of seasonal climate and diurnal precipitation over Central America to land and sea surface schemes in RegCM4. Clim Res 52:31–48

Emanuel KA (1991) A scheme for representing cumulus convection in large-scale models. J Atmos Sci 48:2313–2335

Emanuel KA, Živkovic-Rothman M (1999) Development and evaluation of a convection scheme for use in climate models. J Atmos Sci 56:1766–1782

Gao XJ, Zhao ZC, Ding YH, Huang RH, and others (2001) Climate change due to greenhouse effects in China as simulated by a regional climate model. Adv Atmos Sci 18:1224–1230

Gao XJ, Zhao ZC, Giorgi F (2002) Changes of extreme events in regional climate simulations over East Asia. Adv Atmos Sci 19:927–942

Gao XJ, Shi Y, Giorgi F (2011) A high resolution simulation of climate change over China. Sci Chin Earth Sci 54: 462–472

Giorgi F, Marinucci MR, Visconti G (1990) Use of a limited-area model nested in a general circulation model for regional climate simulation over Europe. J Geophys Res 95:18413–18431

Giorgi F, Marinucci MR, Bates GT (1993a) Development of a second-generation regional climate model (RegCM2). I. Boundary-layer and radiative transfer processes. Mon Weather Rev 121:2794–2813

Giorgi F, Marinucci MR, Bates GT (1993b) Development of a second-generation regional climate model (RegCM2). II. Convective processes and assimilation of lateral boundary conditions. Mon Weather Rev 121:2814–2832

Giorgi F, Francisco R, Pal J (2003) Effects of a subgrid-scale topography and land use scheme on the simulation of surface climate and hydrology. I. Effects of temperature and water vapor disaggregation. J Hydrometeorol 4: 317–333

Giorgi F, Coppola E, Solmon F, and others (2012) RegCM4: Model description and preliminary tests over multiple CORDEX domains. Clim Res 52:7–29

Grell GA (1993) Prognostic evaluation of assumptions used by cumulus parameterizations. Mon Weather Rev 121: 764–787

Gu HH, Wang GL, Yu ZB, Mei R (2012) Assessing future climate changes and extreme indicators in east and south Asia using the RegCM4 regional climate model. Clim Change 114:301–317

Guo DL, Yang MX, Wang HJ (2011) Sensible and latent heat flux response to diurnal variation in soil surface temperature and moisture under different freeze/thaw soil conditions in the seasonal frozen soil region of the central Tibetan Plateau. Environ Earth Sci 63:97–107

Ji ZM, Kang SC (2013) Double-nested dynamical downscaling experiments over the Tibetan Plateau and their projection of climate change under two RCP scenarios. J Atmos Sci 70:1278–1290

Jin J, Miller NL, Schlegel N (2010) Sensitivity study of four land surface schemes in the WRF model. Adv Meteorol 2010:167436, doi:10.1155/2010/167436

Ju L, Wang HJ (2006) A regional climate model nested in a global gridpoint general circulation model. Chin J Geophys 49:49–58 (in Chinese with English abstract)

Ju L, Wang H, Jiang D (2007) Simulation of the Last Glacial Maximum climate over East Asia with a regional climate model nested in a general circulation model. Palaeogeogr Palaeoclimatol Palaeoecol 248:376–390

Kiehl JT, Hack JJ, Bona GB, Boville BA, and others (1996) Description of the NCAR Community Climate Model (CCM3). Technical Report NCAR/TN-420+STR, National Center For Atmospheric Research, Boulder, CO

Laprise R (2008) Regional climate modelling. J Comput Phys 227:3641–3666

Lawrence PJ, Chase TN (2007) Representing a new MODIS consistent land surface in the Community Land Model (CLM 3.0). J Geophys Res 112:G01023, doi:10.1029/2006JG000168

Lee DK, Suh MS (2000) Ten-year east Asian summer monsoon simulation using a regional climate model (RegCM2). J Geophys Res 105:565–577

Li GP (2007) Climatic characteristics of the Tibetan Plateau. In: Li GP (author) Dynamic meteorology of the Tibetan Plateau. China Meteorological Press, Beijing, p 1–4 (in Chinese)

Li Q, Xue YK (2010) Simulated impacts of land cover change on summer climate in the Tibetan Plateau. Environ Res Lett 5:015102, doi:10.1088/1748-9326/5/1/015102

Liu YQ, Giorgi F, Washington W (1994) Simulation of summer monsoon climate over East Asia with NCAR regional climate model. Mon Weather Rev 122:2331–2348

Ma LJ, Zhang TJ, Li Q, Frauenfeld OW, and others (2008) Evaluation of ERA-40, NCEP-1, and NCEP-2 reanalysis air temperatures with ground-based measurements in China. J Geophys Res 113:D115, doi:10.1029/2007JD009549

Ma YM, Wang Y, Wu R, Hu Z, and others (2009) Recent advances on the study of atmosphere-land interaction observations on the Tibetan Plateau. Hydrol Earth Syst Sci 13:1103–1111

Niu GY, Yang ZL (2006) Effects of frozen soil on snowmelt runoff and soil water storage at a continental scale. J Hydrometeorol 7:937–952

Niu GY, Yang ZL, Dickinson RE, Gulden LE (2005) A simple TOPMODEL-based runoff parameterization (SIMTOP) for use in global climate models. J Geophys Res Atmos 110:D21106, doi:10.1029/2005JD006111

Octaviani M, Manomaiphiboon K (2011) Performance of regional climate model RegCM3 over Thailand. Clim Res 47:171–186

Oleson KW, Dai Y, Bonan G, Bosilovich M, and others (2004) Technical description of the Community Land Model. Technical Note NCAR/TN-461+STR, National Center

For Atmospheric Research, Boulder, CO

Oleson KW, Niu G, Yang Z, Lawrence D and others (2007) CLM3.5 documentation. National Center for Atmospheric Research, Boulder, CO

Oleson KW, Niu GY, Yang ZL, Lawrence DM, and others (2008) Improvements to the Community Land Model and their impact on the hydrologic cycle. J Geophys Res 113: G01021, doi:10.1029/2007JD000563

Pal JS, Small EE, Eltahir EAB (2000) Simulation of regional scale water and energy budgets: representation of subgrid cloud and precipitation processes within RegCM. J Geophys Res 105:29579–29594

Pal JS, Giorgi F, Bi X, Elguindi N and others (2007) Regional climate modeling for the developing world: the ICTP RegCM3 and RegCNET. Bull Am Meteorol Soc 88: 1395–1409

Park JH, Oh SG, Suh MS (2013) Impacts of boundary conditions on the precipitation simulation of RegCM4 in the CORDEX East Asia domain. J Geophys Res 118:1–16

Phan VT, Ngo-Duc T, Ho TMH (2009) Seasonal and interannual variations of surface climate elements over Vietnam. Clim Res 40:49–60

Qu P, Yang MX, Guo DL, Chen CX (2009) Simulation of summer air temperature and precipitation over Tibetan Plateau with Regional Climate Model (RegCM3). Plateau Meteorol 28:738–744 (in Chinese with English abstract)

Seneviratne SI, Corti T, Davin EL, Hirschi M, and others (2010) Investigating soil moisture–climate interactions in a changing climate: a review. Earth Sci Rev 99: 125–161

Shi Y, Gao XJ, Wu J, Giorgi F (2011) Changes in snow cover over China in the 21st century as simulated by a high resolution regional climate model. Environ Res Lett 6: 045401, doi:10.1088/1748-9326/6/4/045401

Steiner AL, Pal JS, Rauscher SA, Bell JL, and others (2009) Land surface coupling in regional climate simulations of the West African monsoon. Clim Dyn 33:869–892

Taylor KE (2001) Summarizing multiple aspects of model performance in a single diagram. J Geophys Res 106: 7183–7192

Wang AH, Zeng XB (2012) Evaluation of multireanalysis products with *in situ* observations over the Tibetan Plateau. J Geophys Res 117:D05102, doi:10.1029/2011 JD016553

Wang GX, Hu H, Li T (2009) The influence of freeze–thaw cycles of active soil layer on surface runoff in a permafrost watershed. J Hydrol (Amst) 375:438–449

Wang JM (1999) Land surface process experiments and interaction study in China from HEIFE to IMGRASS and GAME-TIBET/TIPEX. Plateau Meteorol 18:280–294 (in Chinese with English abstract)

Wang NL (2006) The boundary between the northern and southern Tibetan Plateau with different variations in the warm season air temperatures on the decadal time scale. Quaternary Sci 26:165–172 (in Chinese with English abstract)

Wang XJ, Yang MX, Wan GN, Chen XL and others (2013) Qinghai-Xizang (Tibetan) Plateau climate simulation using a regional climate model RegCM3. Clim Res 57: 173–186

Wang Y, Leung LR, McGregor JL, Lee DK and others (2004) Regional climate modeling: progress, challenges, and prospects. J Meteorol Soc Jpn 82:1599–1628

Wu GX, Liu YM, He B, Bao Q and others (2012) Thermal controls on the Asian summer monsoon. Sci Rep 2:404 doi:10.1038/srep00404

Wu J, Gao XJ (2013) A gridded daily observation dataset over China region and comparison with the other datasets. Chin J Geophys 56:1102–1111 (in Chinese with English abstract)

Xu Y, Gao XJ, Shen Y, Xu CH and others (2009) A daily temperature dataset over China and its application in validating a RCM simulation. Adv Atmos Sci 26:763–772

Yang MX, Yao TD, Gou XH, Nozomu H and others (2007a) Diurnal freeze/thaw cycles of the ground surface on the Tibetan Plateau. Chin Sci Bull 52:136–139

Yang MX, Yao TD, Gou XH, Tang H (2007b) Water recycling between the land surface and atmosphere on the northern Tibetan Plateau — a case study at flat observation sites. Arct Antarct Alp Res 39:694–698

Yang YW, Yang MX (2008) Application of Regional Climate Model (RegCM3) to the Tibetan Plateau: sensitivity experiments for cumulus convection parameterization scheme. J Glaciol Geocryol 30:250–258 (in Chinese with English abstract)

Yao TD, Thompson L, Yang W, Yu W and others (2012) Different glacier status with atmospheric circulations in Tibetan Plateau and surroundings. Nat Clim Change 2: 663–667

Yasunari T (2006) Land-atmosphere interaction. In: Wang B (ed) The Asian monsoon. Springer, Berlin, p 459–478

Ye DZ (1979) Introduction. In: Ye DZ, Gao YX (eds) Tibetan plateau meteorology. Science Press, Beijing, p 30–55 (in Chinese)

Zeng X, Zhao M, Dickinson RE (1998) Intercomparison of bulk aerodynamic algorithms for the computation of sea surface fluxes using TOGA COARE and TAO data. J Clim 11:2628–2644

Zeng X, Shaikh M, Dai Y, Dickinson RE, Myneni R (2002) Coupling of the common land model to the NCAR community climate model. J Clim 15:1832–1854

Zhang DF, Gao XJ, Bai HZ (2005) Simulation of climate over Qinghai-Xizang Plateau utilizing RegCM3. Plateau Meteorol 24:714–720 (in Chinese with English abstract)

Zhang JY, Wu LY (2011) Land-atmosphere coupling amplifies hot extremes over China. Chin Sci Bull 56: 3328–3332

Zhang JY, Wu LY, Dong WJ (2011) Land–atmosphere coupling and summer climate variability over East Asia. J Geophys Res 116:D05117

Zhou YW, Guo DX, Qiu GQ, Cheng GD (2000) Geocryology in China. Science Press, Beijing (in Chinese)

Zou J, Xie ZH (2012) The effects of the land-surface process parameterization of the RegCM4 on climate simulation in East Asia. Acta Meteorol Sin 70:1312–1326 (in Chinese with English abstract)

Editorial responsibility: Filippo Giorgi, Trieste, Italy

Submitted: December 29, 2013; Accepted: August 18, 2014
Proofs received from author(s): November 4, 2014